ARTICLE

Effect of Electrode Orientations on Charge Transport in Alkanedithiol Single-Molecule Junctions

Arijit Sen[†] **and Chao-Cheng Kaun**[†,‡,*]

[†]Research Center for Applied Sciences, Academia Sinica, Taipei 11529, Taiwan, and [‡]Department of Physics, National Tsing-Hua University, Hsinchu 30013, Taiwan

ABSTRACT Using first-principles calculations based on the density functional theory and the nonequilibrium Green's functions approach, we study the charge transport in Au—alkanedithiol—Au single-molecule junctions with different electrode orientations and molecular lengths. We attribute the recently measured high-/low-conductance in these heterostructures to two distinct electrode orientations, [100] and [111], which can control the electrode—molecule coupling as well as the tunneling strength by way of diverse band structures. Our detailed analysis on the transmission spectra suggests that even a single alkanedithiol junction can serve as a double quantum-dot system to yield tunable quantum interference.

KEYWORDS: molecular electronics · gold nanowires · electronic transport · double quantum dot · tunable quantum interference · first-principles

Controlling individual molecules to manipulate conventional microelectronics toward hybrid devices and to eventually build novel electronics entirely out of self-assembly is a promising approach in realizing nanoelectronics,[1,2] where single-molecule junctions form the fundamental building blocks.[3−5] Measuring the conductance of such junctions, which is crucial for device development, is often difficult because of complexity in the atomistic details such as contact geometries and molecular conformations. However, through the repetition of thousands of measurements to allow statistical determination, binary (high/low) conductance in alkanedithiol single-molecule junctions has been observed with consistence by various groups.[6−12] These results offer an excellent opportunity to better understand quantum transport in molecular junctions. To date, quantitative agreement between measured and calculated conductance[11,13−15] exists for the high (H) conductance state but not for the low (L) conductance state which is about five times smaller.

Recent theoretical studies[11,14,16] have explained H- and L-conductance[6−12] of the junctions in terms of different contact geometries, namely, atop−hollow and atop−atop, respectively. However, the respective calculated values[11,14] have been five times larger than the measured ones. Furthermore, since the S−Au bond is stronger than the Au−Au bond where the junction breakdown occurs,[6,9] an atop−atop configuration is more feasible than an atop−hollow one.[15] Since the calculated L-conductance from atop−atop configuration[11,14,15] agrees paradoxically with the measured H-conductance, such an outcome may stem from the inadequacy of the density functional theory (DFT)[11] or, alternatively, from the lack of the right junction configuration for the measured L-conductance. Therefore, the origin of the binary conductance in such junctions has remained an open question, which we try to address here.

In the scanning probe microscope break junction measurement, as the gold tip is gradually retracted from the single molecule, topological nanowires form at its end.[17] These nanowires have strong likelihood along the [100] and [111] directions.[18] Since conduction is a result of the carrier flow incident on the devices from electrodes,[19,20] different electrode orientations having different band structures should affect the junction conductance. In view of this, we utilize *first principles* calculations to investigate the effects of two different electrode orientations, [100] and [111], on the conductance of alkanedithiol junctions with three different molecular lengths, hexanedithiol (HDT), octanedithiol (ODT), and decanedithiol (DDT), where the number (N) of the methylene (CH_2) groups varies from 6 to 10. We explain the origin of the

*Address correspondence to kauncc@gate.sinica.edu.tw.

Received for review July 30, 2010 and accepted October 06, 2010.

Published online October 11, 2010. 10.1021/nn101840a

experimentally observed binary conductance of such junctions. Our detailed analysis on the transmission spectra further sheds light on the charge transport processes in such mesoscopic systems.

RESULTS AND DISCUSSION

Figure 1a shows the relaxed junction geometries (see Methods) of HDT bonded to gold adatoms on Au(100) (top panels) and Au(111) (bottom panels) electrodes, when viewed along the *x* axis (left panels) and the *y* axis (right panels). The scattering region forming our simulation box[14] is indicated by a rectangle, which includes a sufficiently large part (about six layers) of the electrodes attached through the adatoms to a single alkanedithiol in between. As Figure 1a suggests, the gold adatoms behave like atomic contacts[21,22] in such heterojunctions, which connect the localized states in the molecule with the propagating states in the continua.

A comparative study of our calculated values of conductance (see Methods) with the available measured data from different laboratories[6,8−11] has been portrayed in Figure 1b, on a natural logarithmic scale as a function of *N*. It turns out that the two distinct electrode orientations, [100] and [111], cater respectively to H- and L-conductance, as they conform well to measured data. In the coherent tunneling regime, the conductance of Au−alkanedithiol−Au systems can be described[23,24] as $G = G_c \exp(-\beta N)$, which yields G_c = 1.11 [0.06]G_0 and β = 1.10 [0.95] for the Au(100) [Au(111)] junctions, in good accord with the literature[6,8−11,23] for the H [L] conductance. To get an idea of the tunneling events, we plot the junction local density of states (LDOS) at E_F in Figure 1c. The LDOS, located at the respective S atoms after being separated from the continua through the gold adatoms, extend into two [one] neighboring C−C bonds [bond] for the Au(100) [Au(111)] junctions. This suggests that the electrode−molecule coupling is stronger for Au(100) junctions than Au(111) ones. As the molecular length increases, the effective tunneling distance (*i.e.*, the distance inside the alkane chain with no LDOS) increases as well. In Figure 1b, there is a good resemblance in the conductance of Au(100)−ODT−Au(100) and Au(111)−HDT−Au(111) and likewise, in the conductance of Au(100)−DDT−Au100 and Au(111)−ODT−Au(111), which are indicated by the horizontal dotted lines. It can be understood from Figure 1c in the sense that the respective effective tunneling distances (denoted by the green and purple arrows) appear to be quite similar in magnitude.

To gain insight into the conduction features, we show in Figure 2 the transmission spectra, $T(E)$, as obtained from our *first-principles* calculations (circles) for junctions of Au(100) (left panels) and Au(111) (right panels) electrodes sandwiching, respectively, HDT (top panels), ODT (middle panels), and DDT (bottom panels).

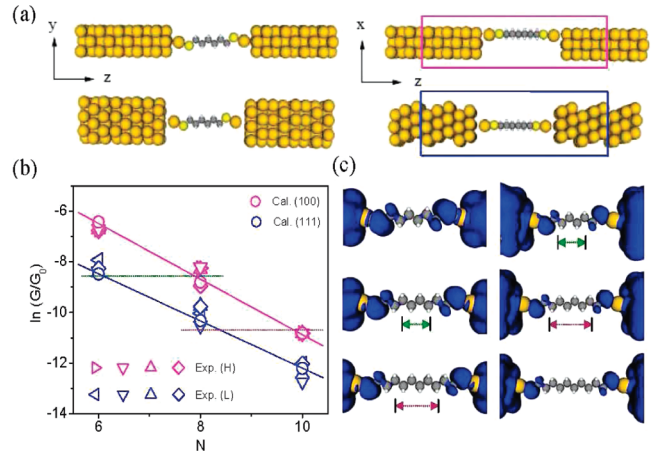

Figure 1. (a) Relaxed junction geometries of hexanedithiol bonded to gold adatoms on Au(100) (top panels) and Au(111) (bottom panels) electrodes, as viewed along the *x* axis (left panels) and the *y* axis (right panels). The scattering region forming our simulation box is indicated by a rectangle. (b) Natural logarithm of conductance *versus* *N* (number of methylene groups, CH_2, in the alkanedithiols) for our calculated results (circles) in comparison with the respective measured data from different laboratories (triangles pointing right,[6] left,[8] down,[9] up,[10] and diamond[11]). The fitted solid lines indicate the exponential decay of conductance as a function of *N* while the horizontal dotted lines refer to the matching of conductance. (c) The local density of states at E_F for both kind of junctions with varying *N*. The green and purple arrows proximate the effective tunneling distances.

The E_F of respective junctions has been set to zero. Each inset shows the transmission profile on a logarithmic scale. We come across two major transmission peaks around E_F in Au(100) [Au(111)] junctions, located

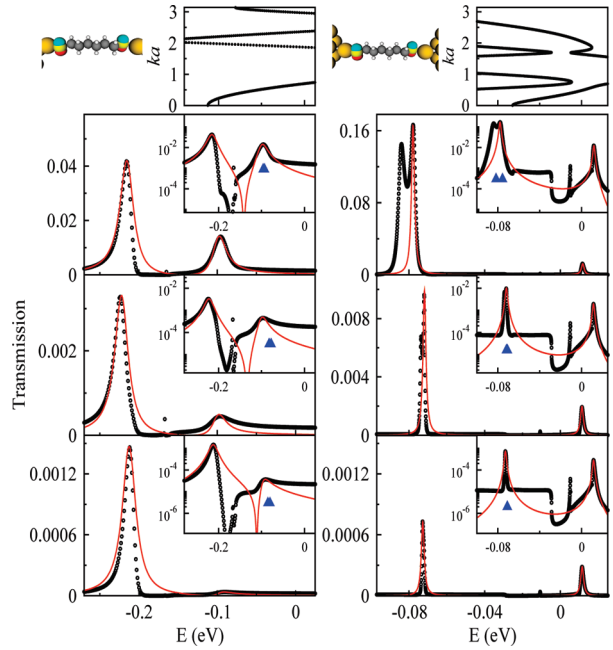

Figure 2. Transmission spectra from *first-principles* calculations (circles) and model analysis (red lines) for junctions of Au(100) (left panels) and Au(111) (right panels) electrodes sandwiching HDT (top panels), ODT (middle panels), and DDT (bottom panels). Each inset shows the transmission profile on a logarithmic scale along with the energy levels of MIGS (triangles). On the top are shown the orbitals of MIGS for Au(100) and Au(111) junctions along with the band structures of respective electrodes.

at around −0.22 and −0.1 [−0.07 and 0.01] eV, and thus separated by about 0.12 [0.08] eV. The immediate peak lying below [above] E_F in the Au(100) [Au(111)] system leads eventually to the hole [electron] mediated off-resonance tunneling. Positions as well as line shapes of the peaks within the same electrode orientation remain almost intact, even for different molecular lengths. However, the relative height of the peaks do change as the molecular length increases, whereas the peak at −0.1 [−0.07] eV diminishes faster than the other peak in Au(100) [Au(111)] junctions. In addition, the fact that the resonance peaks are wider in Au(100) junctions than in Au(111) ones demonstrates that the electrode−molecule coupling in the former is stronger than in the latter, in tune with the observation of Figure 1c. Peculiarity in the shapes of these peaks further suggests that the dominating contribution comes from asymmetric Fano-type resonances in Au(100) junctions, while the contribution is mainly from symmetric Breit−Wigner-type resonances in Au(111) junctions (see refs 25 and 26).

Since both the lowest unoccupied molecular orbital and the highest occupied molecular orbital (HOMO) of an isolated alkanedithiol stay far away[14] from E_F, the metal-induced gap states (MIGS) contribute significantly to the formation of transmission maxima.[27,28,16] We compute the MIGS by diagonalizing the sub-Hamiltonian matrix that includes the alkanedithiol along with two gold adatoms on either side.[29] The two MIGS (as shown by filled triangles in Figure 2) are mostly degenerate, forming the HOMO of the junctions. These are responsible for the onset of one transmission peak located at −0.1 [−0.07] eV for Au(100) [Au(111)] junctions. As the top of Figure 2 suggests, each MIGS having a p_x orbital character is located at either of the two S atoms (viewed along 45° of the x axis).

The one-dimensional band structures of Au(100) and Au(111) electrodes are also shown at the top of Figure 2. The characteristics of these bands play a crucial role in determining the electrode−molecule coupling in respective junctions. In addition, the high density of states at an electrode band edge can transfer more electrons from the electrode to the adjacent S atom, leading to a band-edge induced state (BEIS). An electrode band edge close to the transmission peak at −0.22 [0.01] eV for Au(100) [Au(111)] junctions thus gives rise to the band-edge resonance (see ref 30).

From the molecular orbital analysis and the band structure study, we envisage the localization of electrons at each S atom on either side of the molecule (see Figure 2). Each S atom thus acts as a quantum dot (QD) with two distinct energy levels E_1 and E_2 coming from the MIGS and BEIS for both junctions. This helps us to construct a simplified double quantum-dot (DQD) model as shown schematically in the inset of Figure 3, where one QD has been assumed to have only one energy level (another level is however absorbed into γ_2,

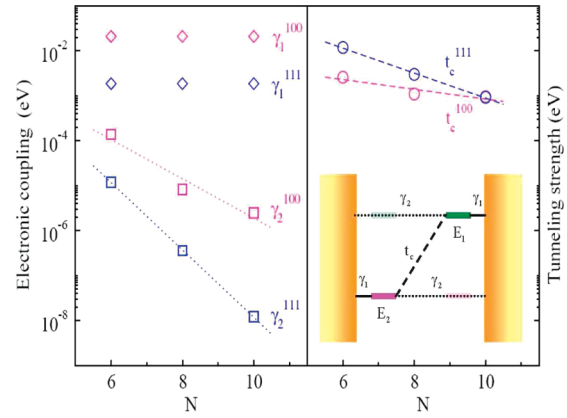

Figure 3. The respective coupling coefficients, γ_1, γ_2, and t_c, for the Au(100) and Au(111) junctions on a logarithmic scale as a function of the molecular length (as extracted from our model analysis following eq 1). Note that γ_1 remains constant in both the cases. The inset shows a schematic illustration of the double quantum-dot model for the molecular junction.

the electrode-QD coupling), so that the molecular junction behaves like a DQD system while coupling to the conduction-band continuum. A similar kind of DQD model formed by two face-to-face benzene molecules was used previously[31] to interpret the complex quantum interference patterns in molecular junctions.[32−34] For γ representing the electrode-QD couplings and t_c being the interdot tunneling strength, the model transmission, $T(E)$, can be obtained as[25]

$$T(E) = \frac{4[t_c\bar{\gamma} - \gamma_{12}(E - \bar{E})]^2}{\left[(E - \bar{E})^2 - \left(\frac{\Delta E}{2}\right)^2 - t_c^2 - \left(\frac{\Delta\gamma}{2}\right)^2\right]^2 + 4[\bar{\gamma}(E - \bar{E}) - t_c\gamma_{12}]^2} \quad (1)$$

where $\bar{E} = (E_1 + E_2)/2$, $\Delta E = E_1 - E_2$, $\bar{\gamma} = (\gamma_1 + \gamma_2)/2$, $\Delta\gamma = \gamma_1 - \gamma_2$, and $\gamma_{12} = (\gamma_1\gamma_2)^{1/2}$. As shown in Figure 2, we have fitted (solid red lines) our calculated transmission spectra (circles) using eq 1. The fitting in the weaker electrode−molecule coupling junction with the Au(111) electrode is better than that in the stronger one with the Au(100) electrode. Since we focus on the two peaks that are closer to E_F, the third peak in the Au(111)−HDT−Au(111) junction (the top-right panel) is not included, which mainly comes from a nearby molecular level. In the insets of the right panel, a part of the transmission profile appears to be flat (below E_F), which may be associated with one particular band having ka around 2 in the Au(111) electrodes. However, our simple model is able to capture the main conduction features in these molecular junctions.

We extract various electronic coupling coefficients regarding the alkanedithiol single-molecule junctions, which are plotted on a logarithmic scale as a function of N in Figure 3. As we see from the schematic illustration of Figure 3, t_c and γ_2 represent the *indirect* and *direct*

tunneling processes for charge carriers to transmit to the other continuum. The resonant suppression of the transmission around −0.17 eV in Au(100) junctions shown in Figure 2 indicates a phase change of π between these two pathways due to destructive quantum interference.[31,35−37] As Figure 2 further suggests, molecular junctions with Au(100) electrode configurations show much more vivid quantum interference between p_x orbitals of MIGS and BEIS, through conduction-electron-tunneling channels, in the form of asymmetric Fano line shapes. This is because both γ_1 and γ_2 are much stronger for Au(100) junctions than for Au(111) junctions. While γ_1 for both kinds of electrodes does not change with an increase in molecular length, t_c and γ_2 happen to cause the reduction in the peak height. However, t_c and γ_2 play different roles in different electrode junctions. In Au(100) [Au(111)] systems, when t_c [γ_2] decreases slightly, the band-edge [MIGS] peak also decreases while the MIGS [band-edge] peak increases. On the other hand, when the reverse happens between t_c and γ_2, both peaks fall off simultaneously. Since the slope of γ_2 is sharper than that of t_c, the MIGS peak decreases faster than the respective band-edge peak. The quantum interference in a molecular junction can therefore be potentially controlled through the electronic coupling either by manipulating the length of molecule or by changing the orientation of the electrode. Since self-assembled alkanedithiol junctions can serve as realistic DQDs in an electronic circuit, it may open up new vistas for future nanoelectronics with accessible control.

CONCLUSIONS

We have shown that Au(100) electrodes can provide the high conductance, while Au(111) electrodes provide the low conductance in alkanedithiol single-molecule junctions, where the majority of charge carriers are, respectively, the holes and the electrons. Our analysis further affirms that a significant influence of the electrode orientation on the molecular conduction can exist through quantum interference. The mutual interplay between the metal-induced gap states and the band-edge induced states through conduction-electron-tunneling channels leads to two dominant transmission peaks close to the Fermi level. The knowledge of various electronic coupling strengths out of a simple double quantum-dot-like model may be used in multiscale modeling aimed at understanding as well as designing futuristic molecular electronic devices.

METHODS

Structural Relaxations. We optimized the junction geometries utilizing DFT[38] within the generalized gradient approximations (GGA).[39] During the optimization, the respective molecule along with two gold adatoms was allowed to move while the other gold atoms (about six layers of the electrodes on each side of it) were kept fixed at the experimental lattice constant of 4.08 Å. We then stretched the distance between the two electrodes, optimized it again, and continued to do so, until the junction broke down. We thus came up with a set of maximally stretched two-probe configurations with minimum energy and also having force within the tolerance limit (0.001 Ry/bohr). At the end, we found that the *atop*−*atop* configuration corresponded to the local minima of the respective free energy in [100] as well as [111] orientations. This agreed well with the experimental observations of the molecular junction breakdown, occurring at the Au−Au bond.[6,9] In addition, the energies/atom of molecular junctions with Au(111) electrodes were found to be lower by about 0.4 eV than those with Au(100) electrodes.

Transport Calculations. First-principles transport calculations were performed using Atomistix ToolKit,[40,41] based on the nonequilibrium Green's functions approach on top of the DFT, within GGA.[39] The scattering region forming our simulation box,[14] as indicated in Figure 1a by a rectangle, included a sufficiently large part (about six layers) of the electrodes attached through the adatoms to a single alkanedithiol in between. The Hamiltonian was expanded in real space having s, p, d double-ζ with a polarization atomic orbital basis set. The atomic cores were defined by the Troullier−Martins pseudopotentials.[42] In the linear response regime, the conductance (G) values were obtained from the Landauer formula, $G = T(E_F)G_0$, where $T(E)$ is the transmission spectrum, E_F is the Fermi energy, and $G_0 = 2e^2/h$ is the quantum of conductance.[43]

Acknowledgment. We thank H. Guo, M.-T. Lee and S.-H. Chang for insightful discussions. This work was partially supported by National Science Council and National Center for Theoretical Sciences, Republic of China.

REFERENCES AND NOTES

1. Joachim, C.; Gimzewski, J. K.; Aviram, A. Electronics Using Hybrid-Molecular and Mono-molecular Devices. *Nature* **2000**, *408*, 541–548.
2. Heath, J. R.; Ratner, M. A. Molecular Electronics. *Phys. Today* **2003**, *56*, 43–49.
3. Nitzan, A.; Ratner, M. A. Electron Transport in Molecular Wire Junctions. *Science* **2003**, *300*, 1384–1389.
4. Tao, N. J. Electron Transport in Molecular Junctions. *Nat. Nanotechnol.* **2006**, *1*, 173–181.
5. Quek, S. Y.; Kamenetska, M.; Steigerwald, M. L.; Choi, H. J.; Louie, S. G.; Hybertsen, M. S.; Neaton, J. B.; Venkataraman, L. Mechanically Controlled Binary Conductance Switching of a Single-Molecule Junction. *Nat. Nanotechnol.* **2009**, *4*, 230–234.
6. Xu, B.; Tao, N. J. Measurement of Single-Molecule Resistance by Repeated Formation of Molecular Junctions. *Science* **2003**, *301*, 1221–1223.
7. González, M. T.; Wu, S.; Huber, R.; van der Molen, S. J.; Schönenberger, C.; Calame, M. Electrical Conductance of Molecular Junctions by a Robust Statistical Analysis. *Nano Lett.* **2006**, *6*, 2238–2242.
8. Jang, S.-Y.; Reddy, P.; Majumdar, A.; Segalman, R. A. Interpretation of Stochastic Events in Single Molecule Conductance Measurements. *Nano Lett.* **2006**, *6*, 2362–2367.
9. Li, X.; He, J.; Hihath, J.; Xu, B.; Lindsay, S. M.; Tao, N. J. Conductance of Single Alkanedithiols: Conduction Mechanism and Effect of Molecule−Electrode Contacts. *J. Am. Chem. Soc.* **2006**, *128*, 2135–2141.
10. Fu, M.-D.; Chen, I.-W. P.; Lu, H.-C.; Kuo, C.-T.; Tseng, W.-H.; Chen, C.-H. Conductance of Alkanediisothiocyanates: Effect of Headgroup-Electrode Contacts. *J. Phys. Chem. C* **2007**, *111*, 11450–11455.
11. Li, C.; Pobelov, I.; Wandlowski, T.; Bagrets, A.; Arnold, A.; Evers, F. Charge Transport in Single Au |Alkanedithiol| Au Junctions: Coordination Geometries and Conformational Degrees of Freedom. *J. Am. Chem. Soc.* **2008**, *130*, 318–326.

12. Zhou, J.; Chen, F.; Xu, B. Fabrication and Electronic Characterization of Single Molecular Junction Devices: A Comprehensive Approach. *J. Am. Chem. Soc.* **2009**, *131*, 10439–10446.
13. Müller, K.-H. Effect of the Atomic Configuration of Gold Electrodes on the Electrical Conduction of Alkanedithiol Molecules. *Phys. Rev. B* **2006**, *73*, 045403.
14. Kaun, C.-C.; Seideman, T. Conductance, Contacts, and Interface States in Single Alkanedithiol Molecular Junctions. *Phys. Rev. B* **2008**, *77*, 033414.
15. Paulsson, M.; Krag, C.; Frederiksen, T.; Brandbyge, M. Conductance of Alkanedithiol Single-Molecule Junctions: A Molecular Dynamics Study. *Nano Lett.* **2009**, *9*, 117–121.
16. Sheng, W.; Li, Z. Y.; Ning, Z. Y.; Zhang, Z. H.; Yang, Z. Q.; Guo, H. Quantum Transport in Alkane Molecular Wires: Effects of Binding Modes and Anchoring Groups. *J. Chem. Phys.* **2009**, *131*, 244712.
17. He, J.; Sankey, O.; Lee, M.; Tao, N. J.; Li, X.; Lindsay, S. Measuring Single Molecule Conductance With Break Junctions. *Faraday Discuss.* **2006**, *131*, 145–154.
18. Rodrigues, V.; Fuhrer, T.; Ugarte, D. Signature of Atomic Structure in the Quantum Conductance of Gold Nanowires. *Phys. Rev. Lett.* **2000**, *85*, 4124.
19. Kaun, C.-C.; Guo, H.; Grütter, P.; Lennox, R. B. Momentum Filtering Effect in Molecular Wires. *Phys. Rev. B* **2004**, *70*, 195309.
20. Luzhbin, D. A.; Kaun, C.-C. Origin of High- and Low-Conductance Traces in Alkanediisothiocyanate Single-Molecule Contacts. *Phys. Rev. B* **2010**, *81*, 035424.
21. Ohnishi, H.; Kondo, Y; Takayanagi, K. Quantized Conductance through Individual Rows of Suspended Gold Atoms. *Nature* **1998**, *395*, 780–783.
22. Yanson, A. I.; Bollinger, G. R.; van den Brom, H. E.; Agrait, N.; van Ruitenbeek, J. M. Formation and Manipulation of a Metallic Wire of Single Gold Atoms. *Nature* **1998**, *395*, 783–785.
23. Joachim, C.; Vinuesa, J. F. Length Dependence of the Electronic Transparence (Conductance) of a Molecular Wire. *Europhys. Lett.* **1996**, *33*, 635–640.
24. Magoga, M.; Joachim, C. Conductance and Transparence of Long Molecular Wires. *Phys. Rev. B* **1997**, *56*, 4722–4729.
25. Ladrón de Guevara, M. L.; Claro, F.; Orellana, P. A. Ghost Fano Resonance in a Double Quantum Dot Molecule Attached to Leads. *Phys. Rev. B* **2003**, *67*, 195335.
26. Papadopoulos, T. A.; Grace, I. M.; Lambert, C. J. Control of Electron Transport through Fano Resonances in Molecular Wires. *Phys. Rev. B* **2006**, *74*, 193306.
27. Kaun, C.-C.; Guo, H. Resistance of Alkanethiol Molecular Wires. *Nano Lett.* **2003**, *3*, 1521–1525.
28. Malen, J. A.; Doak, P.; Baheti, K.; Tilley, T. D.; Segalman, R. A.; Majumdar, A. Identifying the Length Dependence of Orbital Alignment and Contact Coupling in Molecular Heterojunctions. *Nano Lett.* **2009**, *9*, 1164–1169.
29. Larade, B.; Taylor, J.; Zheng, Q. R.; Mehrez, H.; Pomorski, P.; Guo, H. Renormalized Molecular Levels in a Sc3N@C80 Molecular Electronic Device. *Phys. Rev. B* **2001**, *64*, 195402.
30. Madhavan, V.; Chen, W.; Jamneala, T.; Crommie, M. F.; Wingreen, N. S. Local Spectroscopy of a Kondo Impurity: Co on Au(111). *Phys. Rev. B* **2001**, *64*, 165412.
31. Joachim, C.; Gimzewski, J. K.; Tang, H. Physical Principles of the Single-C_{60} Transistor Effect. *Phys. Rev. B* **1998**, *58*, 16407–16417.
32. Sautet, P.; Joachim, C. Electronic Interference Produced by a Benzene Embedded in a Polyacetylene Chain. *Chem. Phys. Lett.* **1988**, *153*, 511–516.
33. Joachim, C.; Gimzewski, J. K. An Electromechanical Amplifier Using a Single Molecule. *Chem. Phys. Lett.* **1997**, *265*, 353–357.
34. Magoga, M.; Joachim, C. Conductance of Molecular Wires Connected or Bonded in Parallel. *Phys. Rev. B* **1999**, *59*, 16011–16021.
35. Solomon, G. C.; Herrmann, C.; Hansen, T.; Mujica, V.; Ratner, M. A. Exploring Local Currents in Molecular Junctions. *Nat. Chem.* **2010**, *2*, 223–228.
36. Rincón, J.; Hallberg, K.; Aligia, A. A.; Ramasesha, S. Quantum Interference in Coherent Molecular Conductance. *Phys. Rev. Lett.* **2009**, *103*, 266807.
37. Ke, S.-H.; Yang, W. Quantum-Interference-Controlled Molecular Electronics. *Nano Lett.* **2008**, *8*, 3257–3261.
38. Giannozzi, P.; Baroni, S.; Bonini, N.; Calandra, M.; Car, R.; Cavazzoni, C.; Ceresoli, D.; Chiarotti, G. L.; Cococcioni, M.; Dabo, I.; *et al.* QUANTUM ESPRESSO: A Modular and Open-Source Software Project for Quantum Simulations of Materials. *J. Phys.: Condens. Matter* **2009**, *21*, 395502.
39. Perdew, J. P.; Burke, K.; Ernzerhof, M. Generalized Gradient Approximation Made Simple. *Phys. Rev. Lett.* **1996**, *77*, 3865.
40. Taylor, J.; Guo, H.; Wang, J. *Ab Initio* Modeling of Quantum Transport Properties of Molecular Electronic Devices. *Phys. Rev. B* **2001**, *63*, 245407.
41. Brandbyge, M.; Mozos, J.-L.; Ordejón, P.; Taylor, J.; Stokbro, K. Density-Functional Method for Nonequilibrium Electron Transport. *Phys. Rev. B* **2002**, *65*, 165401.
42. Troullier, N.; Martins, J. L. Efficient Pseudopotentials for Plane-Wave Calculations. *Phys. Rev. B* **1991**, *43*, 1993–2006.
43. Datta, S. *Electrical Transport in Mesoscopic Systems*; Cambridge University Press: Cambridge, U.K., 1997.